Capsule controlled release of crystallisation inhibitors in mortars

Kamat, Ameya; Palin, Damian; Lubelli, Barbara; Schlangen, Erik

DOI
10.1016/j.matdes.2024.113156

Publication date
2024

Document Version
Final published version

Published in
Materials and Design

Materials & Design 244 (2024) 113156

Contents lists available at ScienceDirect

Materials & Design

journal homepage: www.elsevier.com/locate/matdes

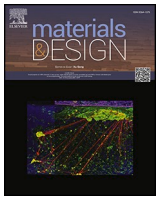

Capsule controlled release of crystallisation inhibitors in mortars

Ameya Kamat [a,b,*], Damian Palin [c], Barbara Lubelli [a], Erik Schlangen [b]

[a] Heritage and Architecture, Architecture and Built Environment, Delft University of Technology, The Netherlands
[b] Materials and Environment, Civil Engineering and Geosciences, Delft University of Technology, The Netherlands
[c] Department of Engineering, University of Cambridge, United Kingdom

ARTICLE INFO

Keywords:
Chitosan-alginate
Polyelectrolyte complex
Ferrocyanide
Salt damage
Leaching
pH responsive

ABSTRACT

Crystallisation inhibitors, such as sodium ferrocyanide (NaFeCN), are highly effective in mitigating NaCl-induced weathering in lime-based mortars; however, direct addition of NaFeCN in lime-mortars increases its susceptibility to leaching and rapid depletion, thus compromising long-term performance. Here, we present hydrogel-capsules for the controlled-release of NaFeCN within hydraulic mortars for the prolonged prevention of salt weathering. Capsules were prepared by complexing chitosan and calcium-alginate in different ratios containing different concentrations of NaFeCN. The release of NaFeCN from these capsules was measured in (1) simulated lime-mortar solution (2) from mortar specimens incorporated with calcium alginate (CA) and chitosan-calcium-alginate (Cs-CA) capsules using ultraviolet–visible light spectrophotometry and Inductive Coupled Plasma-Optical Emission Spectroscopy. Mortars containing Cs-CA capsules exhibited controlled-release of NaFeCN with four times lower effective diffusion coefficient, compared to incorporating NaFeCN directly in mortar. Conversely, mortar containing CA capsules (without chitosan) released NaFeCN rapidly. Thus, chitosan's presence in CA is necessary for tuning NaFeCN release and the reason may be attributed to chitosan's role in reducing CA's permeability and chitosan's electrostatic-attraction to ferrocyanide anions, slowing diffusion of the latter. In conclusion, using Cs-CA capsules can control the release of NaFeCN within mortar, providing a steady NaFeCN supply to prolong mortar's resistance against salt damage.

1. Introduction

The crystallisation of salts within porous building materials is a leading cause of building damage [1]. Salts, particularly sodium chloride (NaCl) from various sources like groundwater, salt spray and de-icing, permeate into building materials through capillary transport [2]. Under supersaturated conditions, salts can exert a crystallisation pressure exceeding the mechanical strength of building materials causing damage [3–5]. Lime-based mortars such as air lime and natural hydraulic lime are a preferred choice for restoration of plasters and renders in the built cultural heritage due to their favourable properties such as high plasticity, high water retention and a better compatibility with existing substrates in comparison to cement-based mortars [6,7]. However, low mechanical strength of lime-based mortars puts them at a higher risk to salt damage. Additionally, exposure of salt-contaminated mortars to fluctuating environmental conditions, including variations in relative humidity and temperature, can result in repeated cycles of dissolution-recrystallisation [8], exacerbating the damage [9]. Lime-mortar-based plasters and renders, particularly those in exposed locations such as building surfaces, are susceptible to damage, necessitating frequent replacement. Frequent repair and replacement costs can be significant. However, these costs can be minimised by improving the durability of repair mortars. In recent decades, the incorporation of crystallisation inhibitors within mortars has yielded promising results in improving mortar durability by altering the process of salt crystallisation [10].

Crystallisation inhibitors are compounds that inhibit crystal nucleation and modify crystal growth by adsorbing onto specific crystal faces [11]. Sodium ferrocyanide decahydrate ($Na_4Fe(CN)_6{\cdot}10H_2O$; hereafter referred to as NaFeCN) is one of the most effective inhibitors of NaCl crystallisation [12]. Hexacyanoferrate(II) ($[Fe(CN)_6]^{4-}$) anions from NaFeCN inhibit and/or delay NaCl nucleation by increasing the critical supersaturation [13]. The $[Fe(CN)_6]^{4-}$ anions sorb onto the {1 0 0} faces of the NaCl crystals, blocking NaCl growth due a difference in the ionic surface charge [14]. This difference results in NaCl crystal growth along the ⟨1 1 1⟩ direction, resulting in the formation of dendritic rather than cubic {1 0 0} crystals [15]. Due to their high surface area, dendritic crystals increase the evaporation rate and promote advection of salt ions

* Corresponding author at: Delft University of Technology, Faculty of Architecture, Julianalaan 134, Delft, 2628BL Delft, The Netherlands.
E-mail address: a.a.kamat@tudelft.nl (A. Kamat).

https://doi.org/10.1016/j.matdes.2024.113156
Received 9 February 2024; Received in revised form 17 June 2024; Accepted 9 July 2024
Available online 10 July 2024

away from the solution [16]. When present in NaCl contaminated porous building materials, the delay in NaCl crystal nucleation and the formation of dendritic crystals allows Na^+ and Cl^- ions to be easily transported towards the evaporative surface where NaCl can crystallise as harmless efflorescence (surface crystallisation) without exerting crystallisation pressure within the pore network [15–19]. In recent years, lime-based mortars incorporating NaFeCN have demonstrated reduced salt damage in laboratory settings [10,20,21] and in the field [22]. Notably, amongst various NaCl inhibitors, NaFeCN remains stable in the alkaline pH range of mortars [23] and does not alter their physical and chemical properties [24,25]. This makes NaFeCN a promising additive for mitigating salt damage in mortars. However, NaFeCN's relatively high solubility (17 % w/w at 25 °C) [26] makes it susceptible to leaching. The depletion of NaFeCN from mortar specimens after repeated wetting–drying cycles has been observed and attributed to the leaching of NaFeCN [20]. A recent systematic study into the leaching behaviour of NaFeCN from mortar specimens incorporating NaFeCN by direct mixing reported severe leaching, concluding that this method of addition may not prevent salt damage in the long run [27]. By slowing down the rate of NaFeCN leaching from mortars it may be possible to prolong their salt damage resistance.

The use of capsules, produced from natural polymer polysaccharides and proteins, for the protection and delivery of various cargoes has gained momentum across a wide range of fields [28–30]. These polymers offer rich functional groups, enabling controlled cargo release and distinct advantages over synthetic polymers, including non-toxicity, abundance, commercial availability, and biodegradability [31]. Alginate, a polysaccharide derived from brown algae [32], exhibits pH-responsive behaviour due to the presence of abundant carboxyl functional groups (–COOH) on its chains. Calcium alginate (CA) capsules, produced through the ionic gelation of sodium alginate (SA) with calcium ions (Ca^{2+}) [33] have long been exploited for controlled drug release in physiological conditions (up to pH 7.4) [34,35]. More recently, CA capsules have been used to encapsulate bacterial spores within highly alkaline concrete (pH ~ 12) for self-healing concrete applications [36,37]. However, the employment of CA capsules for controlled release of cargo within alkaline construction materials may pose some challenges as the –COOH deprotonate becoming negatively charged carboxylate ions (COO^-) [38], resulting in capsule swelling and rapid release of cargo [39]. Additionally, CA has been shown to disintegrate in alkaline conditions [40]. Chitosan (Cs), a cationic biopolymer derived from crustaceans such as shrimps and crabs [41] also demonstrates pH responsiveness due to the presence of amine functional groups ($–NH_2$) on its chains [42]. In highly alkaline conditions, the positively charged ammonium ions ($–NH_3^+$) lose its positive charge resulting in contraction and renders the polymer insoluble [43]. Cs' positive charge attracts net negatively charged ions, such as $[Fe(CN)_6]^{4-}$, allowing Cs capsule's to retain such ions [44]. Furthermore, Cs because of its positive charge can form a polyelectrolyte complex (PEC) with negatively charged alginate [40,45]. Several studies have used this PEC to produce Cs-CA capsules that demonstrated the sustained release of cargo and increased mechanical stability in the biomedical field [46–50]. Cs both limits the swelling of the CA capsules providing a tighter physical barrier for slowing down the release of the cargo [51,52] and reduces the ease of solvation of CA capsules in high pH conditions [40,53]. In the past, attempts have been made to use synthetic pH-responsive capsules in simulated concrete solutions [54], but so far controlled release of cargo using natural polymers like Cs-CA in construction materials have not been explored.

In a preliminary study, we investigated the release of $[Fe(CN)_6]^{4-}$ from Cs-CA capsules in solutions across a range of alkaline pH values (7–13) for the first time [55]. The results suggest that the ratio between Cs and CA can be used to tune $[Fe(CN)_6]^{4-}$ release in alkaline solutions. This raises an interesting question: *Can Cs-CA capsules be used for the controlled release of NaFeCN from within hardened hydraulic lime mortar?* To answer this question, we produce Cs-CA capsules containing NaFeCN and incorporate these capsules within natural hydraulic lime mortar and perform series of experiments to assess the controlled release of NaFeCN from the mortar.

2. Experimental design

To investigate the controlled release of NaFeCN from mortar-capsule system, an experimental plan was devised consisting of three phases: (1) capsule preparation, (2) capsule selection, and (3) capsule-controlled release in mortar (Fig. 1). The results of each phase informing the next phase.

In the initial phase, CA capsules containing NaFeCN were produced through ionic gelation of SA with Ca^{2+}. The subsequent CA capsules were then coated with Cs to obtain Cs-CA capsules. The Cs:SA ratio and the initial concentration of NaFeCN was varied to obtain diverse combinations of capsules.

In the second phase, the morphology of the capsules and encapsulated NaFeCN were characterised. The release of NaFeCN from the capsules was assessed in a synthetic lime mortar pore solution, to mimic conditions within a mortar pore-network. Capsules were selected considering both the rate of release into the pore solution and the total amount of encapsulated NaFeCN.

In the third phase, the selected capsules were incorporated in mortar specimens and the controlled release of NaFeCN was evaluated based on two transport mechanisms: (i) diffusion-driven transport: whereby the effective diffusion coefficient of NaFeCN was measured based on the leaching rate under accelerated conditions; and (ii) Advection-driven transport: by subjecting mortar specimens to cycles of capillary absorption-drying and the transport of NaFeCN was monitored. The advection-driven test simulates realistic field conditions. The results were compared with those for mortar specimens made with directly mixed-in NaFeCN.

3. Materials and methods

3.1. Materials

Sodium alginate (SA, (mannuronic/guluronic ratio (M/G) of 1.56), calcium chloride dihydrate ($CaCl_2{\cdot}2H_2O$), NaCl and Chitosan (Cs, molecular weight (M_w) ranging from 190–310 kDa) were used to prepare the capsules (all from Sigma-Aldrich). Sodium ferrocyanide decahydrate (NaFeCN; Acros organics) was used as the crystallisation inhibitor. Acetic acid (CH_3COOH; J.T. Baker) and sodium hydroxide (NaOH; Honeywell) were also used in the study. Natural hydraulic lime (NHL) with a strength class of 3.5 MPa (from St. Astier, France) and standard river sand (following NEN-EN 196–1 [56]) were used to prepare of mortar specimens.

3.2. Preparation of capsules

3.2.1. Calcium alginate capsules

CA capsules containing NaFeCN were prepared with various compositions (Table1) using ionic gelation technique [33]. In brief, SA (2 % w/v) and NaFeCN were dissolved in demineralised water. The mixture was then extruded into a continuously stirred (300 rpm) gelation bath of $CaCl_2{\cdot}2H_2O$ (3 % w/v) using a peristaltic pump (Masterflex console drive, Cole Parmer instruments) connected to a needle (0.9 mm internal diameter). The mixture forming beads crosslinked with Ca^{2+} in the bath to form CA capsules loaded with NaFeCN. To minimise outward diffusion of NaFeCN from the capsules during production, NaFeCN was also added to the gelation bath with the same concentration as the extruded SA mixture. The obtained CA capsules were washed with demineralised water to remove excess unlinked Ca^{2+} and Na^+ ions and dried at 40 °C for 48 h. Blank CA capsules (CA-blank) were also prepared using the same method but without the inclusion of NaFeCN.

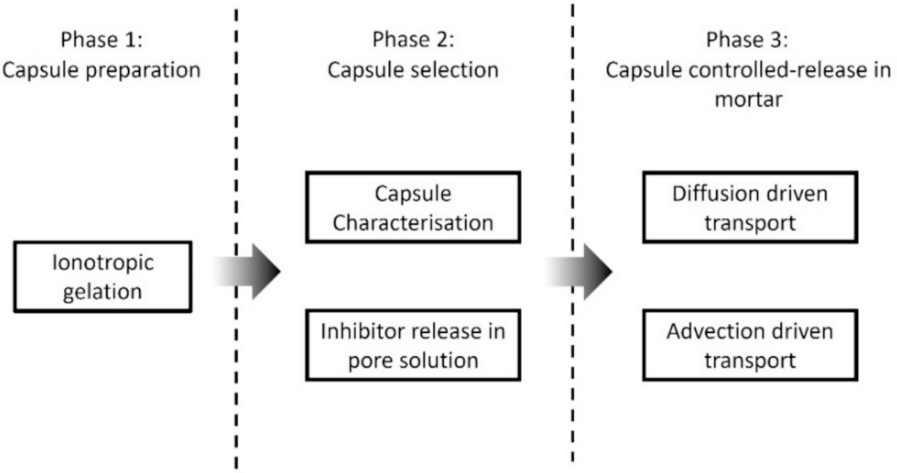

Fig. 1. The experimental design scheme is divided in three phases. The arrow indicates the workflow where results from the preceding phase informs the experimental design of the subsequent phase.

Table 1
Overview of the different capsule types and their composition.

Capsule type	Capsule label	SA % (w/v)	Initial F % (w/v)	Cs % (w/v)	Cs:SA
Calcium alginate blank	CA-blank		–	–	–
Calcium alginate with sodium ferrocyanide	CA-F_2		2	–	–
	CA-F_4		4	–	–
Chitosan-calcium alginate with sodium ferrocyanide	Cs-CA 0.25-F_2	2	2	0.5	0.25
	Cs-CA 0.375-F_2		2	0.75	0.375
	Cs-CA 0.5-F_2		2	1	0.5
	Cs-CA 0.25-F_4		4	0.5	0.25
	Cs-CA 0.375-F_4		4	0.75	0.375
	Cs-CA 0.5-F_4		4	1	0.5

CA = Calcium alginate, F = Sodium ferrocyanide, Cs = Chitosan, SA = Sodium alginate.

3.2.2. Chitosan-coated calcium alginate capsules

Cs-CA capsule with various compositions were prepared (Table 1). A Cs bath was prepared by dissolving Cs in 0.1 M CH_3COOH for 24 h under stirring at 40 °C. Subsequently, wet CA capsules, obtained as described in Section 3.2.1, were added to Cs bath and complexed for 15 min under gentle stirring (300 rpm). Different Cs concentrations within the bath were used to obtain Cs-coated-CA (Cs-CA) capsules with different Cs:SA ratios. Following this, the resulting Cs-CA capsules were washed and dried as above (Section 3.2.1).

3.3. Preparation of mortar specimens

Mortar specimens were prepared by mixing NHL (bulk density 0.69 g mL^{-1}) and sand (bulk density 1.7 g mL^{-1}) in a volumetric ratio of 1:3 with a water-to-binder (w/b) ratio of 1.19. In all the mortar specimens containing capsules, the corresponding dry capsules were first mixed with the dry sand before adding NHL and water. The mortar was mixed in a planetary mixer (Hobart N50-5L) at 140 rpm for a maximum time of 180 s in accordance with [56]. Four specimens types were prepared (Table 2): (i) Mortar-blank: Mortar specimens containing no NaFeCN or capsules; (ii) Mortar-CA-F: Mortar specimens with incorporated CA-F_2 [calcium alginate containing NaFeCN with an initial 2 % (w/v)] capsules such that the total mass of NaFeCN was equivalent to 10 % of the weight of NHL [27]; (iii) Mortar-Cs-CA-F: mortar specimens with incorporated Cs-CA 0.25-F_4 [chitosan-calcium alginate containing NaFeCN with an initial 4 % (w/v)] capsules such that the total mass of NaFeCN was equivalent to 10 % of the weight of NHL; and (iv) Mortar-F: plain mortar specimens containing directly added NaFeCN and CA-blank [calcium alginate containing no NaFeCN] capsules. The Mortar-F specimens were prepared by dissolving NaFeCN (10 % of the weight of NHL) in the mixing water and adding it to sand and NHL. CA-blank capsules were added to Mortar-F mix to obtain a comparable pore size distribution as Mortar-CA-F and Mortar-Cs-CA-F specimen. Note: The type of capsules mixed into the mortar specimens was based on the results of Phase 2 (Section 4.3). All specimens were cylindrical (Φ = 30, H = 50 mm). The specimens were sealed in polyvinyl chloride containers and cured at 20 °C and 95 % RH for 28 days before testing.

3.4. Capsules characterization

The capsules were observed with a digital microscope (Keyence VHX-7000). The dimensions of the capsules were measured using the microscope's in-built software. A minimum of 50 capsules per type were measured along maximum and minimum dimensions. The mean value and the standard deviation were calculated. To quantify the amount of NaFeCN encapsulated within each capsule type, a series of steps were

Table 2
Overview of type of mortar specimens and their mix design. The type and dosage of capsules for each mortar type are also stated.

Mortar specimen label	Label of capsule incorporated	F % (to NHL weight)	Capsule content % (to NHL weight)	NHL:Sand (volumetric ratio)	NHL:Sand (weight ratio)	w/b (weight ratio)
Mortar-blank	–	–	–	1:3	1:7.33	1.19
Mortar-CA-F	CA-F_2	10	32.5	1:3	1:7.33	1.19
Mortar-Cs-CA-F	Cs-CA 0.25-F_4	10	37	1:3	1:7.33	1.19
Mortar-F	CA-blank (containing no F)	10 (added directly)	32.5	1:3	1:7.33	1.19

CA = Calcium alginate, Cs = Chitosan, F = Sodium ferrocyanide, NHL = Natural hydraulic lime, w/b = water-to-binder ratio.

undertaken. The capsules were first milled to a fine powder using a ball mill (Retsch MM200). The powder was then mixed in 1.5 M NaOH solution and subsequently passed through a 0.45 μm syringe membrane. The filtrate was analysed for Fe(II)/(III) concentration using inductive coupled plasma optical emission spectroscopy (ICP-OES; PerkinElmer Optima 5300DV). The amount of NaFeCN (C_{NaFeCN}) is expressed in mg g^{-1} of capsule mass, calculated as:

$$C_{NaFeCN} = \frac{C_{Fe}.(V_{solution}).(Mw_{NaFeCN}/Aw_{Fe})}{M_{sample}} \quad (1)$$

where, C_{Fe} is the measured Fe(II)/(III) concentration in mg L^{-1}, $V_{solution}$ is the volume of NaOH solution in L, M_{sample}= Mass of capsule sample in g. Mw_{NaFeCN}/Aw_{Fe} is the ratio of the molecular weight of NaFeCN to the atomic weight of Fe. Based on stoichiometry, Fe and NaFeCN were assumed to contain the equal number of moles.

3.5. Procedure for assessment of NaFeCN release

3.5.1. NaFeCN release in pore solution

Pore solution was prepared as a binder-slurry filtrate based on the method described by [57]. NHL and demineralised water were mixed in a 2:1 ratio, stirred for 24 h, centrifuged, and the resulting supernatant was vacuum filtered to obtain a clear pore solution. The ionic composition and pH of the solution were analysed by ICP-OES and a pH meter (Metrohm 914), respectively (Table S1, Supplementary info.). 100 mg of each type of capsules (Table 1) was added to 100 mL of the pore solution and stored within airtight plastic containers. Samples of the pore solutions (500 μL) were collected at various time intervals (10 min–1 h) over a 6-hour period. The samples were analysed for NaFeCN content using an ultraviolet–visible (UV–VIS) spectrophotometer (Shimadzu UV2600) at a wavelength of 218 nm [13]. To quantify the content of NaFeCN through UV–VIS, a calibration curve was generated (Fig. S1, Supplementary info.) and the absorbance of the plain pore solution was used as the baseline.

3.5.2. NaFeCN leaching from hardened mortar

3.5.2.1. Diffusion-driven transport. The diffusion-driven transport of NaFeCN from different mortar specimens (Table 2) was assessed in accordance with the accelerated leaching test (ASTM C1308-21) [58], a method previously used to assess NaFeCN leaching from mortar [27]. Each mortar specimen was suspended in a separate cylindrical tank filled with demineralised water as the leachant such that the specimen surface area to leachant volume was 0.15 cm^{-1}. Submerging the specimens facilitated the transport of $[Fe(CN)_6]^{4-}$ ions from the mortar matrix into the leachant. Leachate samples (20 mL) were collected at 2 and 5 h and subsequently every 24 h until day 10 of the test. The samples were analysed for leached $[Fe(CN)_6]^{4-}$ concentration and their pH by UV–VIS and a pH meter, respectively. After the collection of each leachant sample, the leachant was renewed with fresh demineralised water, effectively resetting the $[Fe(CN)_6]^{4-}$ concentration in the leachant to zero. Leachate samples from Mortar-blank specimens were used to create a baseline for UV–VIS measurements. The calibration curve (Fig. S1, Supplementary info.) was used to measure $[Fe(CN)_6]^{4-}$ in the leachate. The concentration of leached $[Fe(CN)_6]^{4-}$ was expressed as cumulative fraction leached (CFL), defined as the ratio of cumulative $[Fe(CN)_6]^{4-}$ amount leached in time to the initial amount of $[Fe(CN)_6]^{4-}$ present in the mortar specimens as stated in ASTM C1308-21 [58]. The effective diffusion coefficient was calculated by fitting CFL data to the analytical solution based on the works of Nestor and Pescatore (Supplementary materials and methods, Supplementary info.) [59,60]. The analytical solution assumes the same boundary conditions as the test setup. Each specimen type was tested in triplicate. To determine the remaining $[Fe(CN)_6]^{4-}$ in the mortar specimens (after the leaching test), a cold water extraction (CWE) was conducted [61]. The test was modified using 1.5 M NaOH as the solvent to release any remaining NaFeCN from the capsules within the specimens. The concentration of Fe ions was measured using ICP-OES and the content of NaFeCN calculated as per Eq. (1). The initial NaFeCN content in each specimen was calculated based on these results and the leaching results (see Supplementary materials and methods, Supplementary info.).

3.5.2.2. Advection-driven transport. The advection-driven transport of three mortar specimen types was tested: Mortar-CA-F, Mortar-Cs-CA-F and Mortar-F (Table 2). The specimens were first dried at 40 °C until reaching a constant weight. The sides of the specimens were sealed using parafilm® (Bemis Company Inc.). The specimens were subjected to three capillary absorption-drying cycles, each cycle consisting of the following steps: saturating the specimens with demineralised water via capillary absorption from the bottom surface; sealing the bottom surface with paraffin film and placing the specimens in a climate chamber for one week at 20 °C, 50 % relative humidity (RH). After one week, the specimens were placed in a drying oven at 40 °C at 15 % RH until reaching a constant weight (typically taking ~ two weeks). Each specimen type was tested in triplicate. At the end of each cycle, images were taken of the drying (top) surface of the specimens using a digital camera.

At the end of the three cycles, two methods were employed to assess the distribution of NaFeCN within the specimens. Firstly, two specimens from each mortar specimen type were dry saw cut in slices measuring 0–5 mm (including efflorescent crust), 5–15 mm, 15–25 mm and 25–50 mm measured from the top surface. The slices were ground into a fine powder using a mortar and pestle. 1 g of the powder was subsampled (using the coning and quartering method [62]) from each slice, which was mixed with 30 mL 1.5 M NaOH (pH 14). Subsequently, the powders were analysed for Fe(II)/(III) (see above, Section 3.4). This procedure was also applied to mortar specimens (two replicates each) that had not been subjected to the leaching test, to assess the initial NaFeCN distribution. For the second method, the third sample from each mortar specimen type was examined using environmental scanning electron microscopy and energy dispersive spectroscopy (ESEM-EDS; FEI quanta 650 FEG, NORAN EDS-Thermo Fischer Scientific) and digital microscopy. For microscopic examination, vertical cross-sections of the specimens (parallel to the direction of the advection-driven transport) were prepared by impregnating the specimen with epoxy resin, saw-cutting the specimens and polishing the saw-cut surface in ethanol (not with water) in accordance with [63]. ESEM was used to image the cross-sections in back-scattered electron (BSE) acquired at 15 keV and EDS was used to map the distribution of Na and Fe as an indicator for NaFeCN, while digital microscopy under plain polarised light was used to obtain images near the evaporative surface with a large field of view.

4. Results

4.1. Characterization of capsules

CA capsules have an ellipsoidal shape with a smooth surface (Fig. 2a, b). The CA-blank capsules are light brown in colour, typical of alginate hydrogels (Fig. 2a). The CA-F_2 capsules are pale yellow in colour and are generally bigger size (volume) than the blank CA capsules (Fig. 2b; Table 3). Notably, the Cs-CA-F_2 capsules have an irregular shape and a rough surface and are bright green in colour (Fig. 2c). The Cs-CA-F 0.25_4 capsules have a similar size as CA-F_2 capsules (Table 3). When CA capsules are added to the Cs bath they tend to agglomerate (Fig. S2, Supplementary information), with the degree of agglomeration increasing with increasing Cs concentration (Section 3.2.2).

Fig. 3 shows the amount of encapsulated NaFeCN in the different types of capsules. The graph shows that capsules with a higher initial concentration of NaFeCN (4 % w/v, red bars) have a higher ultimate NaFeCN content as compared to capsules with a lower initial concentration (2 % w/v, blue bars). Notably, in the case of the Cs-CA 0.25

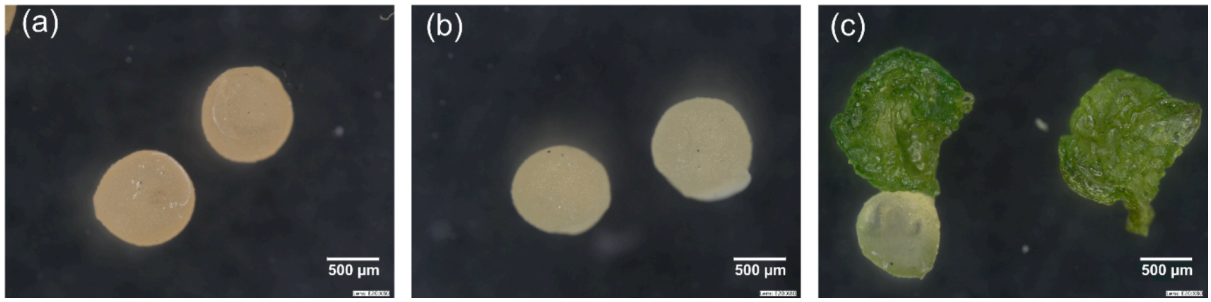

Fig. 2. Digital microscope images of three capsule types after drying: (a) CA-blank: a calcium alginate capsule containing no NaFeCN; (b) CA-F_2: a calcium alginate capsule made with an initial concentration of 2% NaFeCN (w/v); and (c) Cs-CA 0.25-F_4: A Chitosan-calcium alginate capsule made with an initial concentration of 4% NaFeCN.

Table 3
The diameter of capsules along two dimensions, with the mean values and standard deviations reported.

Capsule label	Maximum diameter (μm)	Minimum diameter (μm)
CA-blank	853.7 ± 66.85	709.3 ± 81.99
CA-F_2	1080 ± 90.4	860.27 ± 110.75
Cs-CA 0.25-F_4	1063 ± 124	730 ± 85.5

CA = Calcium alginate, F = sodium ferrocyanide, Cs = Chitosan.

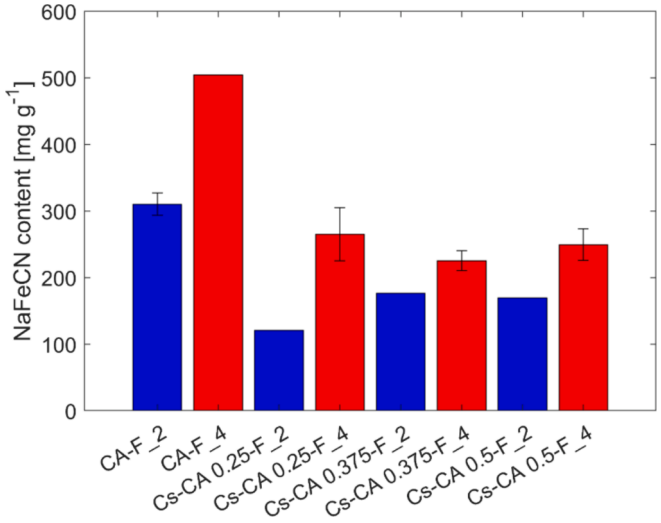

Fig. 3. Encapsulated NaFeCN content expressed in mg g^{-1} of capsule weight. Higher initial NaFeCN concentration (4%) leads to higher encapsulated NaFeCN content in capsules. The blue bars represent capsules produced with an initial concentration of NaFeCN of 2% (w/v), while the red bars represent capsules produced with an initial NaFeCN concentration of 4% (w/v).

capsules, increasing the initial concentration of NaFeCN from 2 % to 4 % (w/v), results in a doubling of the NaFeCN content in the capsules. However, in the case of capsules with higher Cs:SA ratios (i.e., Cs-CA 0.375 and Cs-CA 0.5), this increase in the initial content shows only a marginal rise in the ultimate NaFeCN content. Interestingly, all Cs-CA capsules with initial NaFeCN concentration of 4 % (w/v), contain similar ultimate NaFeCN content (i.e. ~ 280–300 mg g^{-1} of capsule weight), independent of the Cs:SA ratio.

4.2. NaFeCN release in pore solution

Fig. 4 shows the release of NaFeCN from different capsules. The amount of NaFeCN released from the capsules depends on the initial NaFeCN content of capsules (Fig. 3). Capsules containing a higher initial

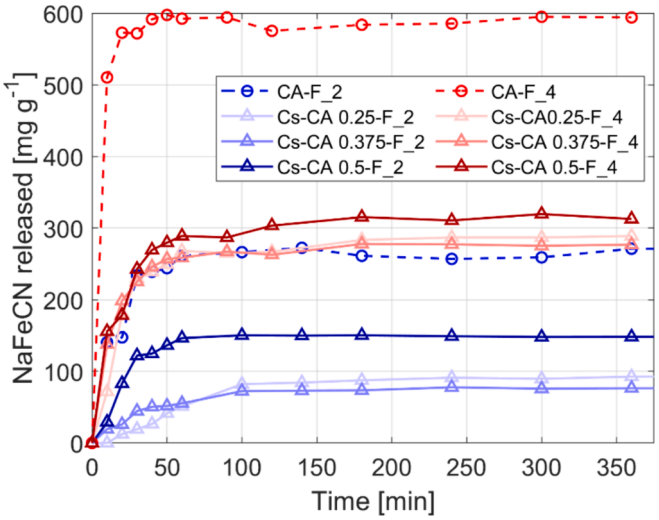

Fig. 4. Graph showing the release profiles of NaFeCN over time from different capsules into a pore solution, expressed as mg g^{-1} of capsule. The blue lines represent capsules made with an initial NaFeCN concentration of 2% (w/v), while the red lines represent capsules with an initial NaFeCN concentration of 4% (w/v). CA capsules are represented by dashed lines and Cs-CA capsules with solid lines.

NaFeCN concentration of 4 % (w/v; Fig. 4, red lines) released a significantly greater amount of NaFeCN as compared to the capsules containing an initial lower 2 % (w/v; Fig. 4, blue lines). Furthermore, the rate of release (i.e., the slope of the of the linear part of the curve) of NaFeCN also depends on their initial NaFeCN content: a higher initial NaFeCN content leads to a higher (or faster) rate of release. For example, CA-F_4 capsules having the highest NaFeCN content released 90 % of their content within the first 10 min. In contrast, Cs-CA 0.25-F_2 capsules with the lowest NaFeCN content took 90 min to release 90 % of their content.

4.3. Selection of the type of capsules for mixing in mortar

An ideal mortar with encapsulated salt inhibitor system is the one that contains sufficient salt inhibitor to inhibit salt crystallisation and release it slow enough to prolong its effectiveness over an extended period. The capsule composition plays a key role on its release rate. Different parameters such as the initial concentration of NaFeCN and the Cs content on Cs-CA capsules were tested to obtain the most suitable capsule type. In the NaFeCN release test in pore solution (Section 4.2), capsules containing low initial content of NaFeCN (2 % w/v) released NaFeCN at a slower rate as compared to capsules containing higher content (4 % w/v capsules, Fig. 4). This difference is due to differences in the concentration gradients between the two capsules and the

leachant (pore solution). The higher the gradient the faster the rate of diffusive release from the capsules [64]. However, Cs-CA capsules made with 2 % (w/v) NaFeCN (~100–150 mg g^{-1} of capsule weight) incorporate significantly lower amount of NaFeCN as compared to Cs-CA capsules with 4 % (w/v; ~280–300 mg g^{-1} of capsule weight). Past research suggests that the concentration of NaFeCN in mortar should be equivalent to ~ 1 % of the binder weight to be effective against salt damage [20]. To achieve sufficient dosage of NaFeCN in mortar, twice as many Cs-CA capsules containing 2 % (w/v) NaFeCN would be required as compared to Cs-CA capsules containing 4 % (w/v) NaFeCN. Increasing the amount of capsules within the mortar will have a negative effect on its mechanical performance due to additional air voids and weak interface transition zones between the mortar matrix and the capsules [65]. Based on the above considerations Cs-CA capsules with high initial NaFeCN content (4 % capsules) are preferable to capsules with lower content (2 % capsules).

Varying the Cs:SA ratio had minimal impact on the encapsulated NaFeCN content as well as its release rate from Cs-CA capsules containing 4 % NaFeCN (Figs. 3 and 4). Cs is comparatively more expensive than CA, making capsules with the lowest Cs content is more cost-effective to produce while still offering comparable release performance compared to Cs-CA capsules with higher Cs:SA ratios (Fig. 4). Furthermore, increasing the Cs content in the production of Cs-CA capsules leads to agglomeration (Fig. S2) which could be problematic for industrial production. Taking these factors into consideration, Cs-CA capsules with high NaFeCN but low Cs content, i.e. Cs-CA 0.25-F_4, were selected as the most suitable for mixing in mortar. CA-F_2, which have a similar NaFeCN content as Cs-CA 0.25 −F_4, were also selected for mixing in mortar to compare NaFeCN leaching from mortar when using Cs-coated versus uncoated capsules (Phase 3, Fig. 1).

4.4. NaFeCN release (leaching) in mortar

4.4.1. Diffusion-driven leaching

The capsules were distributed homogeneously in the mortar matrix and were able to survive the mortar mixing process (see Fig. S7, Supplementary materials and methods). The diffusion-driven leaching of NaFeCN from mortar specimens over time is presented in Fig. 5a. The Mortar-CA-F specimens exhibit a comparable leaching rate to the Mortar-F specimens, showing that CA capsules do not reduce leaching from mortar. In contrast, Mortar-Cs-CA-F specimens demonstrate a slower rate of NaFeCN leaching as compared to Mortar-F specimens. The measured mean effective diffusion coefficient of NaFeCN from Mortar-Cs-CA-F (1.1×10^{-7} cm^2 s^{-1}) is four times lower than that of Mortar-F (4.5×10^{-7} cm^2 s^{-1}). Moreover, at the end of 10-days, the amount of NaFeCN leached from the Mortar-Cs-CA-F specimens drops to just 46.2 %, while for the Mortar-Cs-CA-F it is almost 80 % (Fig. 5a and S3). Furthermore, the NaFeCN release from Mortar-Cs-CA-F does not reach a plateau, indicating a sustained release even after 10 days of accelerated testing. The pH measurements on the leachate show an initial increase of pH until first 24 h, followed by a linear decrease in the pH with every renewal step (Fig. 5b). The drop in pH is consistent across all types of specimens.

4.4.2. Advection-driven leaching

Advection-driven leaching leads to the formation of an efflorescent crust on the drying surface (top surface) of the mortar specimens (Fig. 6, Figs. S4–S6). Mortar-F specimens show crust formation immediately after one absorption-drying cycle, and each cycle leads to a progressive accumulation of the crust. In contrast, the Mortar-CA-F and Mortar-Cs-CA-F specimens display negligible crust formation after the first two absorption-drying cycles. At the end of third cycle, Mortar-CA-F and Mortar-Cs-CA-F show signs of crust formation. In the case of Mortar-Cs-CA-F specimens, the crust is accumulated in localised pockets (Fig. 6, right column, bottom row; marked with black arrows), while Mortar-F and Mortar-CA-F show homogenous crust formation over their entire surface. Visually, after three cycles, the total amount of crust formation on the drying surface is highest for Mortar-F and least for Mortar-Cs-CA-F specimens. Examination of the cross-sections of the Mortar-F, Mortar-CA-F and Mortar Cs-CA-F specimens by digital microscopy shows accumulation of white precipitates just below the drying surface (~0–5 mm depth; Fig. 7 (a-c)). SEM-EDS maps made in these locations reveal the presence of Fe and Na indicating that these precipitates are likely to be NaFeCN crystals (Fig. 7 (d–l)).

The initial distribution of NaFeCN across all mortar specimen types, namely Mortar-F, Mortar-CA-F and Mortar-Cs-CA-F fall within a similar concentration range (before cycling; Fig. 8a). The distribution profile of NaFeCN over the specimen height as measured with ICP-OES on the milled slices of the specimens at the end of the test, underwent a drastic change from a homogenous initial distribution (before cycling; Fig. 8a) to a skewed distribution near the top drying surface (Fig. 8b). At the end of the test, a large amount of NaFeCN is transported and accumulated within the first 5 mm below the drying surface and a depletion in the lower depths (5–50 mm). In the first 5 mm, the mean concentration of NaFeCN for Mortar-Cs-CA-F (33.9 mg g^{-1}) is about half than that of Mortar-F (66.62 mg g^{-1}) and Mortar-CA-F (71.63 mg g^{-1}). In the depths,

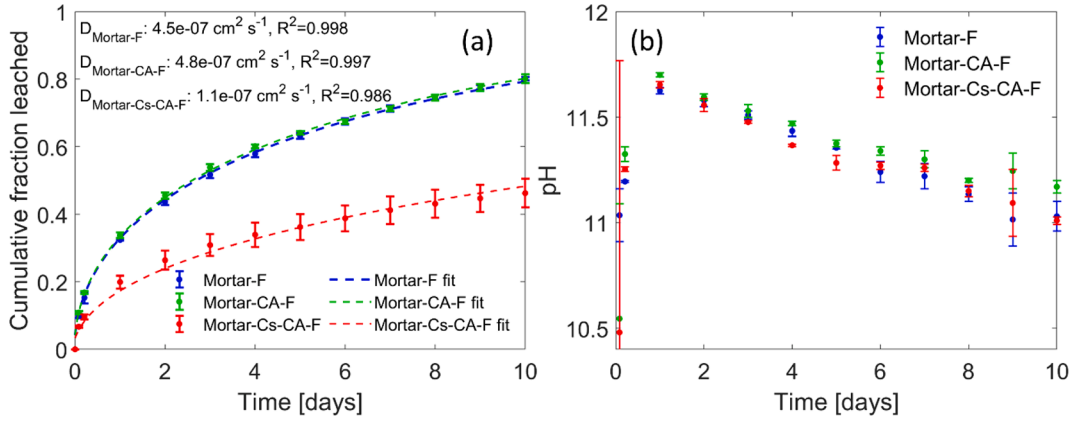

Fig. 5. (a) A plot showing the cumulative fraction leached of sodium ferrocyanide (NaFeCN) measured from hardened mortar specimens at specific time steps during the diffusion driven-accelerated leaching test. The cumulative fraction leached is the ratio of the total NaFeCN leached with respect to the initial amount at the start of the test. The dotted lines represent the best fit curves obtained from the analytical solution (Supplementary materials and methods, Supplementary info.) and their corresponding diffusion coefficients, D, with coefficient of determination (R^2), calculated from the best fit are presented in the top left of the plot. (b) pH measurements of the leachate containing NaFeCN measured at ever time step before leachant renewal. The pH shows a decreasing trend over time in a similar range across all mortar specimens. The error bars indicate one standard deviation from the mean measurements.

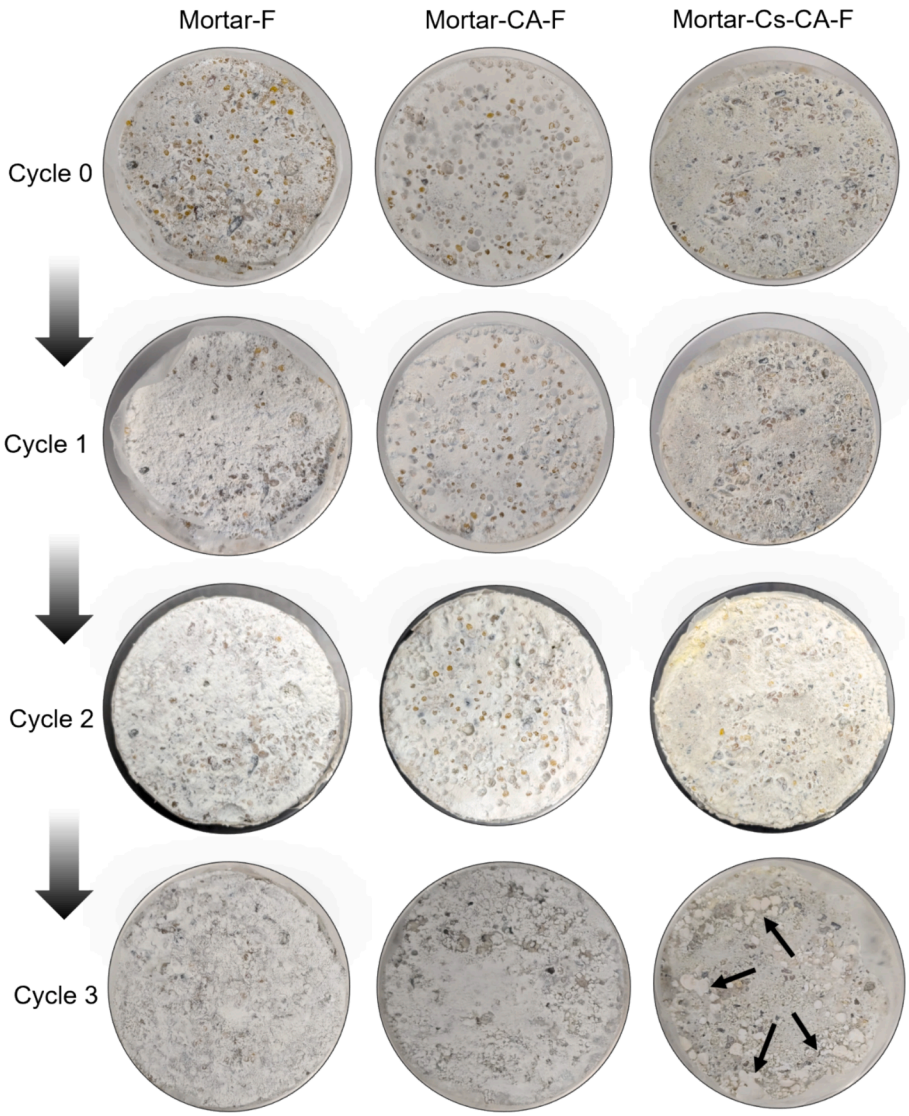

Fig. 6. Images of Mortar-F, Mortar-CA-F and Mortar-Cs-CA-F showing the progression of a white precipitated crust (efflorescence) on the top surface of the specimens after each absorption-drying cycle. The crust formation increases with each cycle.

there is a negligible difference in the final concentration of NaFeCN measured across all specimen types (~8–11 mg g^{-1}).

5. Discussion

The results from diffusion-driven leaching test on mortar specimens show that Mortar-Cs-CA-F specimens [containing Cs-CA capsules containing NaFeCN], exhibit an effective diffusion coefficient of NaFeCN four times lower than Mortar-F [containing directly added NaFeCN] and Mortar-CA-F specimens [containing CA capsules containing NaFeCN], respectively (Fig. 5a). The improved performance of Cs-CA capsules can be attributed to physico-chemical changes induced by the incorporation of Cs. The addition of Cs to CA is known to reduce permeability of CA [51,52] and improve mechanical stability of CA network in alkaline conditions [40]. This is achieved by the ability of Cs to restrict the swelling of CA networks in high pH environments [39,43], possibly due to strong attractive forces between Cs and alginates that prevents repulsion between alginate chains [66], thereby forming tight low porosity networks. A tighter, more stable Cs-CA structure makes it physically more difficult for a small molecule like NaFeCN to escape the capsule matrix [67]. Additionally, Chitosan is also chemically functional due to its positively charged $–NH_2$, which electrostatically interact with negatively charged $[Fe(CN)_6]^{4-}$ ions [68]. Indirect evidence of this interaction can be seen as the green colour of the Cs-CA capsules (Fig. 2c) related to a formation of an ammonium ferrocyanide bond [69] and the agglomeration of the capsules in presence of $[Fe(CN)_6]^{4-}$ as reported in this study (Fig. S2). The $–NH_2$ of Cs capsules acting as chelating sites for $[FeCN_6]^{4-}$ ions have been shown to retain $[FeCN_6]^{4-}$ ions inside the capsule network [44]. Furthermore, attractive forces due to oppositely charged electrostatic interactions between the matrix and the solute have been shown to hinder diffusion of charged solute species [70]. The electrostatic interaction between $[FeCN_6]^{4-}$ ions to Cs is pH dependent and reversible. At high pH, the binding affinity of Cs for $[FeCN_6]^{4-}$ is low due to Cs's neutral charge; however, this affinity increases as the pH decreases [71]. The mortar leaching experiment with mortar specimens containing Cs-CA capsules aligns with this pH-dependant behaviour. The mortar-Cs-CA-F specimens exhibit lower cumulative leaching over time (Fig. 5a) as the pH decreases (Fig. 5b). Realistically, NHL mortars in the field are also expected to carbonate over time causing a slow drop in pH. This slow drop could contribute towards a slower release of $[FeCN_6]^{4-}$ for longer time periods. It must be noted, however, that at very high pH (pH > 12), the $–NH_2$ can become negatively charged by losing protons and releasing bound $[FeCN_6]^{4-}$ ions due to repulsion as observed in [72]. Measuring changes to the

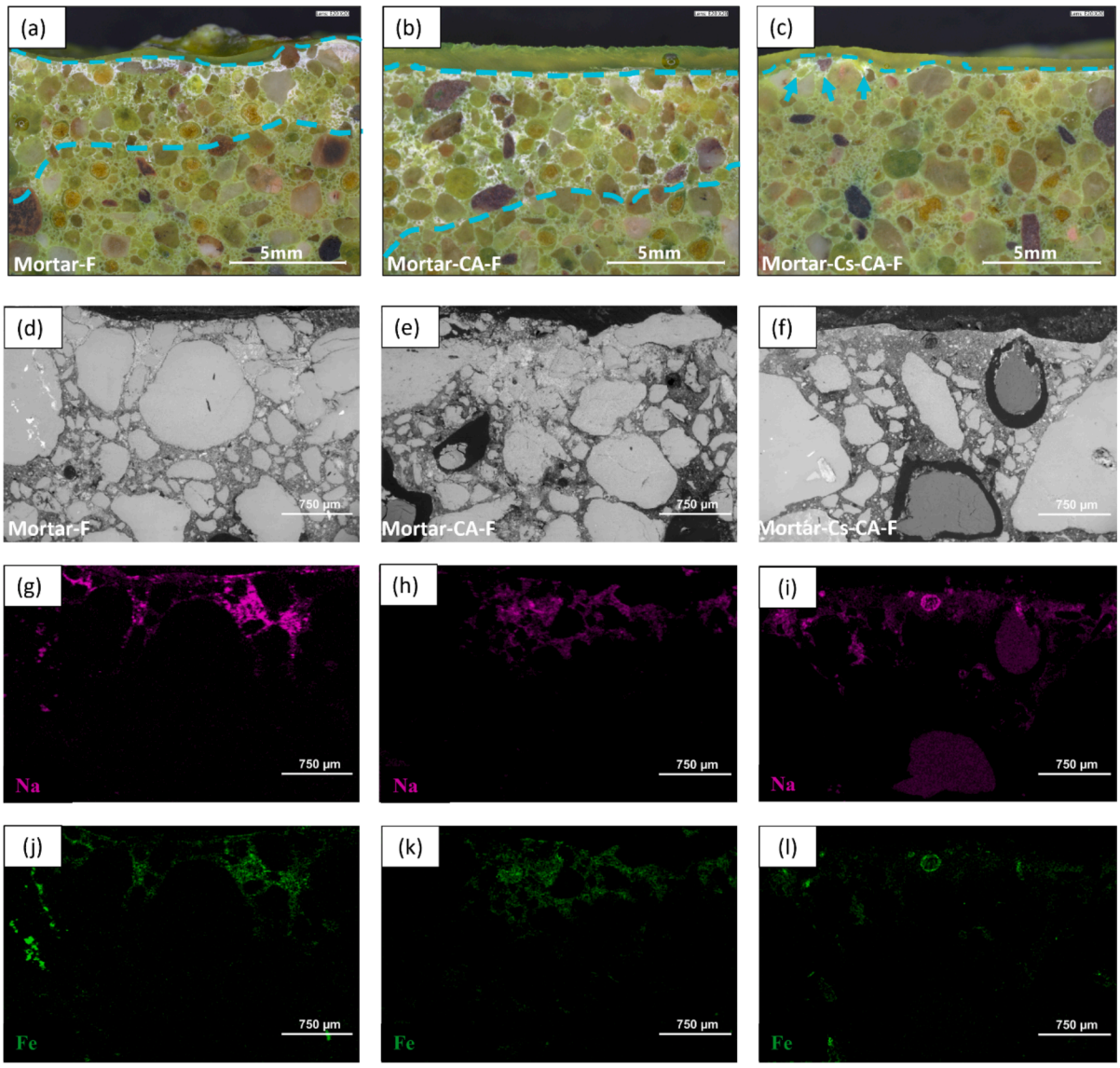

Fig. 7. (a–c) Digital microscope images showing an epoxy-impregnated polished cross-section of: (a) Mortar-F specimen; (b) Mortar-CA-F specimen; and (c) Mortar-Cs-CA-F specimen, at the end of the adsorption and drying test. The field of view presents the top evaporative surface of these mortar specimens. The extent of precipitation is marked with cyan lines. (d–f) Back scattered electron (BSE) images and (g–l) energy dispersive spectroscopy (EDS) maps of polished cross section of Mortar-F (d,g,j), Mortar-CA-F (e,h,h) and Mortar-Cs-CA-F (f,i,l) specimens respectively are corresponding regions of interest from (a–c). The top of the image is the top edge of the cross-section. The grey scale BSE images show accumulation of light grey precipitates in between the sand aggregates. Na and Fe maps of these BSE images indicate the phase to be NaFeCN. The contrast of Na and Fe maps is exaggerated for better visibility and can be used only qualitatively.

surface charge of the capsules using tools, such as Zeta-potential mapping [73] and AFM [74] will help clarify the electrostatic interactions between the $[FeCN_6]^{4-}$ ions and the functional groups on the capsule surface.

The results from the advection-driven leaching test show a notable delay in the transport of NaFeCN towards the drying surface of Mortar-Cs-CA-F and Mortar-CA-F as compared to Mortar-F specimens (Fig. 6). The reason for this delay may be attributed to a limited moisture accessibility. In contrast to the diffusion-driven test setup, where the specimens remain completely saturated, in the advection-driven test, the specimens are only saturated for a short period during the capillary absorption phase and the moisture decreases during the drying phase. In Mortar-F specimens where NaFeCN is already present in the mortar matrix, NaFeCN readily dissolves and is transported to the drying surface even with a limited supply of moisture in the first cycle itself. Conversely, in Mortar-CA-F and Mortar-Cs-CA-F specimens, availability of moisture for a limited time may not be sufficient to swell the hydrogel networks and release enough $[FeCN_6]^{4-}$ ions from the capsules, thereby delaying the $[FeCN_6]^{4-}$ transport. At the end of the test, after three absorption-drying cycles, the effect of slow transport of NaFeCN towards the drying surface (top surface) in Mortar-Cs-CA-F specimens is more evident than Mortar-CA-F specimens (Fig. 6, 7). The distribution profile of NaFeCN at the end of the test confirms this observation as it shows that NaFeCN concentration near the drying surface (0–5 mm; Fig. 8b) in mortar-Cs-CA-F is almost two times lower than that of Mortar-CA-F and Mortar-F. The results show that the presence of Cs is necessary to delay the release of $[FeCN_6]^{4-}$ ions from CA capsules when subjected to successive absorption-drying cycles. However, considering the mass conservation between the NaFeCN distribution profile before cycling (Fig. 8a) and after the test (Fig. 8b), one would expect a higher concentration of NaFeCN in the depths of Mortar-Cs-CA-F specimen, but instead a similar depletion of the NaFeCN concentration is observed in Mortar-F and Mortar-CA-F specimens. While the reason for this discrepancy is unclear, one possible reason could be that a portion of

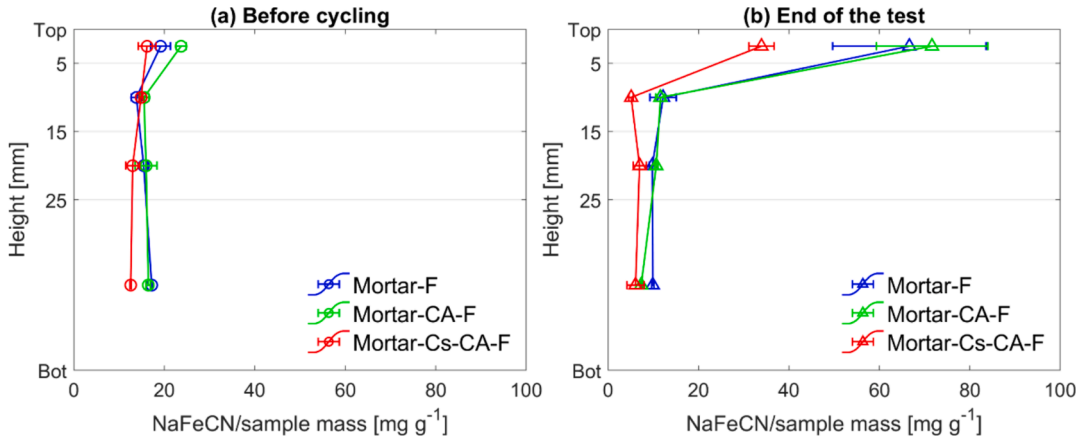

Fig. 8. Plots showing the distribution profile of NaFeCN over specimen height. (a) before subjecting specimens to the absorption-drying cycles and (b) after subjecting them to three cycles (at the end of the test). Depth is measured as the distance from the top of the specimen surface, as indicated in the Y-axis, Top indicates the top of the specimens (0 mm) and Bot indicates the bottom (50 mm). Measurements were taken at four discrete points using ICP-OES on samples obtained after slicing the specimens using a dry saw between: 0–5 mm, 5–15 mm, 15–25 mm and 25–50 mm. The most significant change in the distribution profile occurs between measurements taken at start and the end of the test in the layer between 0–5 mm.

NaFeCN remains bound to Cs due to electrostatic interaction and is not fully released, leading to lower measured NaFeCN values. A high degree of immobilisation of NaFeCN to Cs could be a challenge when applying this technology, as it could limit the availability of NaFeCN. However, it can be overcome in the future by making use of ionic cross-linking agents such as sodium tripolyphosphate that can compete with $[FeCN_6]^{4-}$ ions for $-NH_2$ sites on Cs [75].

The results from mortar leaching tests clearly show that Cs-CA capsules reduce the rate of NaFeCN leaching under both diffusion and advection driven transport as compared to directly adding NaFeCN to mortar. When moisture supply is limited, both Cs-CA and CA capsules tend to release NaFeCN slower in mortar matrix as compared to NaFeCN directly mixed in mortar due to the physical barrier presented by the capsule network. However, when a continuous moisture supply is available, CA capsules may swell releasing more NaFeCN and the effect of capsule's physical barrier is diminished. Conversely, Cs-CA capsules, with cationic Cs, swell less providing a physical barrier for the $[FeCN_6]^{4-}$ anions. Additionally, functional groups on Cs show pH-dependent electrostatic attraction to $[FeCN_6]^{4-}$ ions, hindering their diffusion from the capsule network causing slower release.

The capsules can be further optimised and fine-tuned for specific applications by controlling physical properties of capsules such as porosity and permeability of capsules by varying the molecular weight of chitosan and the M/G ratio of alginates [40]. Use of other cross-linking agents such as sodium tripolyphosphate can also reduce pore diameters and promote better cargo entrapment during production [75]. Modification of Cs such as N-trimethyl chitosan chloride can alter the pH range for protonation to release various charged cargos such as $[FeCN_6]^{4-}$ at specific pH's [43,76].

The Cs-CA capsules developed in this study offer a range of new possibilities for the controlled release of charged molecules in construction materials. For instance they could be used for the controlled release of corrosion inhibitors [77] that need a slow/delayed release to be effective or as an alternative to existing capsule technologies for delivering chemical retarders such as sucrose in controlling cement hydration [78]. Additionally, the bio-based nature of the capsules makes them a sustainable alternative to synthetic polymers [31]. Furthermore, the immobilisation property of Cs-CA capsules could find application in preventing heavy metal leaching from municipal solid waste incineration fly ash which is a promising supplementary cementitious material, but poses an environmental hazard due to the leaching of toxic heavy metals [79,80].

6. Conclusions and outlook

This study introduces a proof-of-concept chitosan-calcium alginate capsule designed for the controlled release of a salt crystallisation inhibitor (NaFeCN) with the aim of prolonging the service life of salt-resistant mortars for renovation and construction applications. This study has shown that NaFeCN can be encapsulated in CA capsules and its release can be controlled by complexing CA with Cs. The results from this study demonstrate that incorporation of Cs is necessary for improving the performance of CA capsules in the alkaline conditions of mortar. The Cs coated CA capsules slow leaching of NaFeCN by reducing the effective diffusion coefficient of NaFeCN from the mortar capsule system (Mortar-Cs-CA-F) compared to adding NaFeCN directly to mortar (Mortar-F). Under advection driven transport that is more commonly observed in field conditions, Cs coated CA capsules reduce and/or delay the leaching of NaFeCN with successive absorption-drying cycles.

The controlled release of NaFeCN from the mortar-capsule system offers advantages, including the ability to provide a steady supply of NaFeCN over a prolonged period of time and lower wastage of NaFeCN due to leaching. Consequently, this technology has the potential to improve the durability of mortars against salt-related damage thereby reducing long-term repair costs. The next step of this research will focus on evaluating the performance of mortars containing Cs-CA-F capsules in resisting NaCl damage under accelerated salt weathering conditions. Additionally, the interactions between NaCl and the capsules needs to be explored, considering past research indicating that high concentrations of NaCl (Na^+:Ca^{2+}>25:1) may compromise the integrity of CA networks [38,81] and might affect the release behaviour of NaFeCN.

CRediT authorship contribution statement

Ameya Kamat: Writing – original draft, Visualization, Methodology, Investigation, Formal analysis, Conceptualization. **Damian Palin:** Writing – review & editing, Supervision, Methodology, Conceptualization. **Barbara Lubelli:** Writing – review & editing, Supervision, Project administration, Methodology, Funding acquisition, Conceptualization. **Erik Schlangen:** Writing – review & editing, Project administration, Methodology, Funding acquisition, Conceptualization.

Declaration of competing interest

The authors declare that they have no known competing financial interests or personal relationships that could have appeared to influence

the work reported in this paper.

Data availability

Data will be made available on request.

Acknowledgments

The research was funded by NWO (Dutch research council) under the project 'MORISAL' (Grant no. 17636). The authors would like to thank Mr. John van den berg, Mrs. Patricia van den Bos and Mrs. Jane Erkmeij for performing ICP measurements, Mr. Arjan Thijssen for ESEM imaging and Ir. Hans Dalderop (TU Eindhoven) for assisting with UV-VIS. Special thanks to Dr. Xu Shi and Dr. Amir Tabakovic (TNO) for providing access to an additional drying oven, without which large scale production of capsules would have been impossible. The authors are grateful to Dr. Leo Pel (TU Eindhoven) and Mr. Armand Middeldorp (TU Delft, water-lab) for providing access to lab facilities at the respective labs.

Appendix A. Supplementary data

Supplementary data to this article can be found online at https://doi.org/10.1016/j.matdes.2024.113156.

References

[1] A. Goudie, H. Viles, Salt weathering hazards, John Wiley & Sons Ltd, Chichester, 1997.
[2] A.E. Charola, Salts in the Deterioration of Porous Materials : An Overview, J. Am. Inst. Conserv. 39 (2000) 327–343, https://doi.org/10.1179/019713600806113176.
[3] G.W. Scherer, Crystallization in pores, Cem. Concr. Res. 29 (1999) 1347–1358, https://doi.org/10.1016/S0008-8846(99)00002-2.
[4] R.J. Flatt, Salt damage in porous materials: how high supersaturations are generated, J. Cryst. Growth 242 (2002) 435–454, https://doi.org/10.1016/S0022-0248(02)01429-X.
[5] M. Steiger, Crystal growth in porous materials - I: The crystallization pressure of large crystals, J. Cryst. Growth 282 (2005) 455–469, https://doi.org/10.1016/j.jcrysgro.2005.05.007.
[6] B.A. Silva, A.P. Ferreira Pinto, A. Gomes, Natural hydraulic lime versus cement for blended lime mortars for restoration works, Constr. Build. Mater. 94 (2015) 346–360, https://doi.org/10.1016/j.conbuildmat.2015.06.058.
[7] K. Elert, C. Rodriguez-Navarro, E.S. Pardo, E. Hansen, O. Cazalla, Lime mortars for the conservation of historic buildings, Stud. Conserv. 47 (2002) 62–75, https://doi.org/10.1179/sic.2002.47.1.62.
[8] J. Desarnaud, N. Shahidzadeh-Bonn, Salt crystal purification by deliquescence/crystallization cycling, EPL (Europhys. Lett.) 95 (2011) 48002, https://doi.org/10.1209/0295-5075/95/48002.
[9] B. Lubelli, R.P.J. van Hees, C.J.W.P. Groot, The effect of environmental conditions on sodium chloride damage: A step in the development of an effective weathering test, Stud. Conserv. 51 (2006) 41–56, https://doi.org/10.1179/sic.2006.51.1.41.
[10] B. Lubelli, T.G. Nijland, R.P.J. Van Hees, A. Hacquebord, Effect of mixed in crystallization inhibitor on resistance of lime-cement mortar against NaCl crystallization, Constr. Build. Mater. 24 (2010) 2466–2472, https://doi.org/10.1016/j.conbuildmat.2010.06.010.
[11] C. Rodriguez-Navarro, L.G. Benning, Control of crystal nucleation and growth by additives, Elements 9 (2013) 203–209, https://doi.org/10.2113/gselements.9.3.203.
[12] A.A.C. Bode, S. Jiang, J.A.M. Meijer, W.J.P. Van Enckevort, E. Vlieg, Growth inhibition of sodium chloride crystals by anticaking agents: In situ observation of step pinning, Cryst. Growth Des. 12 (2012) 5889–5896, https://doi.org/10.1021/cg3012537.
[13] A. Glasner, M. Zidon, The crystallization of NaCl in the presence of [Fe(CN)6]4- ions, J. Cryst. Growth 21 (1974) 294–304, https://doi.org/10.1016/0022-0248(74)90018-9.
[14] A.A.C. Bode, V. Vonk, F.J. Van Den Bruele, D.J. Kok, A.M. Kerkenaar, M. F. Mantilla, S. Jiang, J.A.M. Meijer, W.J.P. Van Enckevort, E. Vlieg, Anticaking activity of ferrocyanide on sodium chloride explained by charge mismatch, Cryst. Growth Des. 12 (2012) 1919–1924, https://doi.org/10.1021/cg201661y.
[15] C. Rodriguez-Navarro, L. Linares-Fernandez, E. Doehne, E. Sebastian, Effects of ferrocyanide ions on NaCl crystallization in porous stone, J. Cryst. Growth 243 (2002) 503–516, https://doi.org/10.1016/S0022-0248(02)01499-9.
[16] S. Gupta, K. Terheiden, L. Pel, A. Sawdy, Influence of Ferrocyanide Inhibitors on the Transport and Crystallization Processes of Sodium Chloride in Porous Building Materials, Cryst. Growth Des. 12 (2012) 3888–3898, https://doi.org/10.1021/cg3002288.
[17] C. Selwitz, E. Doehne, The evaluation of crystallization modifiers for controlling salt damage to limestone, J. Cult. Herit. 3 (2002) 205–216, https://doi.org/10.1016/S1296-2074(02)01182-2.
[18] B. Lubelli, R.P.J. van Hees, Effectiveness of crystallization inhibitors in preventing salt damage in building materials, J. Cult. Herit. 8 (2007) 223–234, https://doi.org/10.1016/j.culher.2007.06.001.
[19] T. Rivas, E. Alvarez, M.J. Mosquera, L. Alejano, J. Taboada, Crystallization modifiers applied in granite desalination: The role of the stone pore structure, Constr. Build. Mater. 24 (2010) 766–776, https://doi.org/10.1016/j.conbuildmat.2009.10.031.
[20] S.J.C. Granneman, B. Lubelli, R.P.J. van Hees, Effect of mixed in crystallization modifiers on the resistance of lime mortar against NaCl and Na2SO4 crystallization, Constr. Build. Mater. 194 (2019) 62–70, https://doi.org/10.1016/j.conbuildmat.2018.11.006.
[21] J. Feijoo, D. Ergenç, R. Fort, M.A. de Buergo, Addition of ferrocyanide-based compounds to repairing joint lime mortars as a protective method for porous building materials against sodium chloride damage, Mater. Struct. 54 (2021) 14, https://doi.org/10.1617/s11527-020-01596-4.
[22] B. Lubelli, E. des Bouvrie, T.G. Nijland, A. Kamat, Plasters with mixed-in crystallization inhibitors: Results of a 4-year monitoring of on-site application, J. Cult. Herit. 59 (2023) 10–22, https://doi.org/10.1016/j.culher.2022.10.016.
[23] T. Páez, A. Martínez-Cuezva, J. Palma, E. Ventosa, Revisiting the cycling stability of ferrocyanide in alkaline media for redox flow batteries, J. Power Sources 471 (2020) 228453, https://doi.org/10.1016/j.jpowsour.2020.228453.
[24] S.J.C. Granneman, B. Lubelli, R.P.J. Van Hees, Characterization of lime mortar additivated with crystallization modifiers, Int. J. Archit. Herit. 12 (2018) 849–858, https://doi.org/10.1080/15583058.2017.1422570.
[25] A. Kamat, B. Lubelli, E. Schlangen, Effect of a mixed-in crystallization inhibitor on the properties of hydraulic mortars, AIMS Mater. Sci. 9 (2022) 628–641, https://doi.org/10.3934/matersci.2022038.
[26] J.A.N. Friend, J.E. Townley, R.H. Vallance, CCCIII.—The solubility of sodium ferrocyanide in water between 0° and 104°, J. Chem. Soc. (1929) 2326–2330, https://doi.org/10.1039/JR9290002326.
[27] A. Kamat, B. Lubelli, E. Schlangen, Leaching behaviour of a crystallisation inhibitor in mortars, J. Build. Eng. 79 (2023) 107933, https://doi.org/10.1016/j.jobe.2023.107933.
[28] J. Li, D.J. Mooney, Designing hydrogels for controlled drug delivery, Nat. Rev. Mater. 1 (2016) 1–18, https://doi.org/10.1038/natrevmats.2016.71.
[29] A.P. Esser-Kahn, S.A. Odom, N.R. Sottos, S.R. White, J.S. Moore, Triggered release from polymer capsules, Macromolecules 44 (2011) 5539–5553, https://doi.org/10.1021/ma201014n.
[30] Y. Yang, Y. Ren, W. Song, B. Yu, H. Liu, Rational design in functional hydrogels towards biotherapeutics, Mater. Des. 223 (2022) 111086, https://doi.org/10.1016/j.matdes.2022.111086.
[31] N. Behabtu, S. Kralj, Enzymatic Polymerization Routes to Synthetic-Natural Materials: A Review, ACS Sustain. Chem. Eng. 8 (2020) 9947–9954, https://doi.org/10.1021/acssuschemeng.0c01664.
[32] H.H. Tønnesen, J. Karlsen, Alginate in drug delivery systems, Drug Dev. Ind. Pharm. 28 (2002) 621–630, https://doi.org/10.1081/DDC-120003853.
[33] E.-S. Chan, B.-B. Lee, P. Ravindra, D. Poncelet, Prediction models for shape and size of ca-alginate macrobeads produced through extrusion–dripping method, J. Colloid Interface Sci. 338 (2009) 63–72, https://doi.org/10.1016/j.jcis.2009.05.027.
[34] A. Shilpa, S.S. Agrawal, A.R. Ray, Controlled Delivery of Drugs from Alginate Matrix, J. Macromol. Sci. Part C Polym. Rev. 43 (2003) 187–221, https://doi.org/10.1081/MC-120020160.
[35] R. Bernasconi, E. Mauri, A. Rossetti, S. Rimondo, R. Suriano, M. Levi, A. Sacchetti, S. Pané, L. Magagnin, F. Rossi, 3D integration of pH-cleavable drug-hydrogel conjugates on magnetically driven smart microtransporters, Mater. Des. 197 (2021), https://doi.org/10.1016/j.matdes.2020.109212.
[36] D. Palin, V. Wiktor, H.M. Jonkers, A bacteria-based bead for possible self-healing marine concrete applications, Smart Mater. Struct. 25 (2016) 084008, https://doi.org/10.1088/0964-1726/25/8/084008.
[37] J. Wang, A. Mignon, D. Snoeck, V. Wiktor, S. Van Vliergerghe, N. Boon, N. De Belie, Application of modified-alginate encapsulated carbonate producing bacteria in concrete: A promising strategy for crack self-healing, Front. Microbiol. 6 (2015) 1–14, https://doi.org/10.3389/fmicb.2015.01088.
[38] W.R. Gombotz, S.F. Wee, Protein release from alginate matrices, Adv. Drug Deliv. Rev. 31 (1998) 267–285, https://doi.org/10.1016/S0169-409X(97)00124-5.
[39] L. Agüero, D. Zaldivar-Silva, L. Peña, M. Dias, Alginate microparticles as oral colon drug delivery device: A review, Carbohydr. Polym. 168 (2017) 32–43, https://doi.org/10.1016/j.carbpol.2017.03.033.
[40] M. George, T.E. Abraham, Polyionic hydrocolloids for the intestinal delivery of protein drugs: Alginate and chitosan - a review, J. Control. Release 114 (2006) 1–14, https://doi.org/10.1016/j.jconrel.2006.04.017.
[41] I. Hamed, F. Özogul, J.M. Regenstein, Industrial applications of crustacean by-products (chitin, chitosan, and chitooligosaccharides): A review, Trends Food Sci. Technol. 48 (2016) 40–50, https://doi.org/10.1016/j.tifs.2015.11.007.
[42] M. Rinaudc, G. Pavlov, J. Desbrières, Solubilization of Chitosan in Strong Acid Medium, Int. J. Polym. Anal. Charact. 5 (1999) 267–276, https://doi.org/10.1080/10236669908009742.
[43] T.W. Wong, Alginate graft copolymers and alginate-co-excipient physical mixture in oral drug delivery, J. Pharm. Pharmacol. 63 (2011) 1497–1512, https://doi.org/10.1111/j.2042-7158.2011.01347.x.
[44] L. Zemskova, A. Egorin, E. Tokar, V. Ivanov, Chitosan-based biosorbents: immobilization of metal hexacyanoferrates and application for removal of cesium

radionuclide from aqueous solutions, J. Sol-Gel Sci. Technol. 92 (2019) 459–466, https://doi.org/10.1007/s10971-019-05019-x.
[45] M. Duran, A. Serrano, A. Nikulin, J.L. Dauvergne, L. Derzsi, E. Palomo del Barrio, Microcapsule production by droplet microfluidics: A review from the material science approach, Mater. Des. 223 (2022) 111230, https://doi.org/10.1016/j.matdes.2022.111230.
[46] G. Pasparakis, N. Bouropoulos, Swelling studies and in vitro release of verapamil from calcium alginate and calcium alginate-chitosan beads, Int. J. Pharm. 323 (2006) 34–42, https://doi.org/10.1016/j.ijpharm.2006.05.054.
[47] A.K. Anal, W.F. Stevens, Chitosan-alginate multilayer beads for controlled release of ampicillin, Int. J. Pharm. 290 (2005) 45–54, https://doi.org/10.1016/j.ijpharm.2004.11.015.
[48] I. Hassan, A. Gani, Alginate-Based pH-Sensitive Hydrogels Encoated with Chitosan as a Bioactive Cargo Carrier with Caffeic Acid as a Model Biomolecule, ACS Food Sci. Technol. 2 (2022) 667–672, https://doi.org/10.1021/acsfoodscitech.1c00466.
[49] Y. Murata, T. Maeda, E. Miyamoto, S. Kawashima, Preparation of chitosan-reinforced alginate gel beads - effects of chitosan on gel matrix erosion, Int. J. Pharm. 96 (1993) 139–145, https://doi.org/10.1016/0378-5173(93)90221-Z.
[50] C. Zhang, X. Wang, M. Xiao, J. Ma, Y. Qu, L. Zou, J. Zhang, Nano-in-micro alginate/chitosan hydrogel via electrospray technology for orally curcumin delivery to effectively alleviate ulcerative colitis, Mater. Des. 221 (2022) 110894, https://doi.org/10.1016/j.matdes.2022.110894.
[51] M.A.S. Santos, M.T.C. Machado, Coated alginate–chitosan particles to improve the stability of probiotic yeast, Int. J. Food Sci. Technol. 56 (2021) 2122–2131, https://doi.org/10.1111/ijfs.14829.
[52] A.D. Sezer, J. Akbuga, Release characteristics of chitosan treated alginate beads: I. Sustained release of a macromolecular drug from chitosan treated alginate beads, J. Microencapsul. 16 (1999) 195–203, https://doi.org/10.1080/026520499289176.
[53] A.J. Ribeiro, C. Silva, D. Ferreira, F. Veiga, Chitosan-reinforced alginate microspheres obtained through the emulsification/internal gelation technique, Eur. J. Pharm. Sci. 25 (2005) 31–40, https://doi.org/10.1016/j.ejps.2005.01.016.
[54] Y. Zhu, Y. Ma, Q. Yu, J. Wei, J. Hu, Preparation of pH-sensitive core-shell organic corrosion inhibitor and its release behavior in simulated concrete pore solutions, Mater. Des. 119 (2017) 254–262, https://doi.org/10.1016/j.matdes.2017.01.063.
[55] A. Kamat, D. Palin, B. Lubelli, E. Schlangen, Tunable chitosan-alginate capsules for a controlled release of crystallisation inhibitors in mortars, MATEC Web Conf. 378 (2023) 02011, https://doi.org/10.1051/matecconf/202337802011.
[56] NEN-EN 196-1: Methods of testing cement - Part 1: Determination of strength, 2015.
[57] C. Schröfl, V. Mechtcherine, M. Gorges, Relation between the molecular structure and the efficiency of superabsorbent polymers (SAP) as concrete admixture to mitigate autogenous shrinkage, Cem. Concr. Res. 42 (2012) 865–873, https://doi.org/10.1016/j.cemconres.2012.03.011.
[58] ASTM C1308-21: Standard test method for accelerated leach test for measuring contaminant releases from solidified waste, 2021. https://doi.org/10.1520/C1308-21.2.
[59] C.W.J. Nestor, Diffusion from solid cylinders, Oak Ridge, TN (United States), 1980. https://doi.org/10.2172/5780257.
[60] C. Pescatore, Improved expressions for modeling diffusive, fractional cumulative leaching from finite-size waste forms, Waste Manage. 10 (1990) 155–159, https://doi.org/10.1016/0956-053X(90)90120-A.
[61] G. Plusquellec, M.R. Geiker, J. Lindgård, J. Duchesne, B. Fournier, K. De Weerdt, Determination of the pH and the free alkali metal content in the pore solution of concrete: Review and experimental comparison, Cem. Concr. Res. 96 (2017) 13–26, https://doi.org/10.1016/j.cemconres.2017.03.002.
[62] ASTM D6323-19: Standard Guide for Laboratory Subsampling of Media Related to Waste Management Activities, 2019. https://doi.org/10.1520/D6323-19.2.
[63] C. Nunes, A. Maria Aguilar Sanchez, S. Godts, D. Gulotta, I. Ioannou, B. Lubelli, B. Menendez, N. Shahidzadeh, Z. Slížková, M. Theodoridou, Experimental research on salt contamination procedures and methods for assessment of the salt distribution, Constr. Build. Mater. 298 (2021) 123862, https://doi.org/10.1016/j.conbuildmat.2021.123862.
[64] A. Mun, H. Simaan Yameen, G. Edelbaum, D. Seliktar, Alginate hydrogel beads embedded with drug-bearing polycaprolactone microspheres for sustained release of paclobutrazol, Sci. Rep. 11 (2021) 1–12, https://doi.org/10.1038/s41598-021-90338-9.
[65] J.Y. Wang, H. Soens, W. Verstraete, N. De Belie, Self-healing concrete by use of microencapsulated bacterial spores, Cem. Concr. Res. 56 (2014) 139–152, https://doi.org/10.1016/j.cemconres.2013.11.009.
[66] M.M. Daly, D. Knorr, Chitosan-Alginate Complex Coacervate Capsules: Effects of Calcium Chloride, Plasticizers, and Polyelectrolytes on Mechanical Stability, Biotechnol. Prog. 4 (1988) 76–81, https://doi.org/10.1002/btpr.5420040205.
[67] J.A.A.D. Sezer, Release characteristics of chitosan treated alginate beads: II. Sustained release of a low molecular drug from chitosan treated alginate beads, J. Microencapsul. 16 (1999) 687–696, https://doi.org/10.1080/026520499288636.
[68] C.A. Rodrigues, E. Stadler, M.C.M. Laranjeira, V. Drago, The preparation and characterization of the hexacyanides immobilized in chitosan, J. Braz. Chem. Soc. 8 (1997) 7–11, https://doi.org/10.1590/S0103-50531997000100003.
[69] J. Luo, B. Hu, C. Debruler, Y. Bi, Y. Zhao, B. Yuan, M. Hu, W. Wu, T.L. Liu, Unprecedented Capacity and Stability of Ammonium Ferrocyanide Catholyte in pH Neutral Aqueous Redox Flow Batteries, Joule. 3 (2019) 149–163, https://doi.org/10.1016/j.joule.2018.10.010.
[70] O. Lieleg, R.M. Baumgärtel, A.R. Bausch, Selective filtering of particles by the extracellular matrix: An electrostatic bandpass, Biophys. J. 97 (2009) 1569–1577, https://doi.org/10.1016/j.bpj.2009.07.009.
[71] Y. Zhang, Y. Thomas, E. Kim, G.F. Payne, PH- and voltage-responsive chitosan hydrogel through covalent cross-linking with catechol, J. Phys. Chem. B 116 (2012) 1579–1585, https://doi.org/10.1021/jp210043w.
[72] N.L. Avery, W. Fries, Selective Removal of Cyanide from Industrial Waste Effluents with Ion-Exchange Resins, Prod. R&d. 14 (1975) 102–104, https://doi.org/10.1021/i360054a009.
[73] C. He, Y. Hu, L. Yin, C. Tang, C. Yin, Effects of particle size and surface charge on cellular uptake and biodistribution of polymeric nanoparticles, Biomaterials 31 (2010) 3657–3666, https://doi.org/10.1016/j.biomaterials.2010.01.065.
[74] J. Joshi, S.V. Homburg, A. Ehrmann, Atomic Force Microscopy (AFM) on Biopolymers and Hydrogels for Biotechnological Applications—Possibilities and Limits, Polymers (Basel). 14 (2022), https://doi.org/10.3390/polym14061267.
[75] M.L. Pita-López, G. Fletes-Vargas, H. Espinosa-Andrews, R. Rodríguez-Rodríguez, Physically cross-linked chitosan-based hydrogels for tissue engineering applications: A state-of-the-art review, Eur. Polym. J. 145 (2021), https://doi.org/10.1016/j.eurpolymj.2020.110176.
[76] Z. Yaneva, D. Ivanova, N. Nikolova, M. Tzanova, The 21st century revival of chitosan in service to bio-organic chemistry, Biotechnol. Biotechnol. Equip. 34 (2020) 221–237, https://doi.org/10.1080/13102818.2020.1731333.
[77] T.A. Söylev, M.G. Richardson, Corrosion inhibitors for steel in concrete: State-of-the-art report, Constr. Build. Mater. 22 (2008) 609–622, https://doi.org/10.1016/J.CONBUILDMAT.2006.10.013.
[78] L. Dong, Y. Zhang, Y. Guo, X. Shu, X. Shen, Q. Ran, P. Feng, Effects of controlled release silica nanocapsules containing sucrose on the heat release of cement hydration, Colloids Surfaces A Physicochem. Eng. Asp. 670 (2023) 131593, https://doi.org/10.1016/j.colsurfa.2023.131593.
[79] H. Luo, Y. Cheng, D. He, E.H. Yang, Review of leaching behavior of municipal solid waste incineration (MSWI) ash, Sci. Total Environ. 668 (2019) 90–103, https://doi.org/10.1016/j.scitotenv.2019.03.004.
[80] B. Chen, P. Perumal, M. Illikainen, G. Ye, A review on the utilization of municipal solid waste incineration (MSWI) bottom ash as a mineral resource for construction materials, J. Build. Eng. 71 (2023) 106386, https://doi.org/10.1016/j.jobe.2023.106386.
[81] R. Vreeker, L. Li, Y. Fang, I. Appelqvist, E. Mendes, Drying and rehydration of calcium alginate gels, Food Biophys. 3 (2008) 361–369, https://doi.org/10.1007/s11483-008-9087-2.